Symbol Rate Processing for the Downlink of DS-CDMA Systems

Michael Joham, *Student Member, IEEE,* and Wolfgang Utschick, *Member, IEEE*

***Abstract*—Many services of third–generation (3G) mobile radio systems will have higher data rates in the downlink than in the uplink. We propose to utilize adaptive antennas at the base stations because spatial interference suppression is able to reduce the near–far effect in the downlink of single-user detection direct-sequence (DS) code division multiple access (CDMA) systems. Besides the channel parameters in terms of directions of arrival, delays, and medium-term average path attenuations which are estimated in the uplink, we also take into account the correlation properties of the spreading and scrambling codes. In DS-CDMA, the users are distinguished by different spreading codes, which change over time due to scrambling. In Brunner et al., the beamforming vectors at the base station were computed slotwise, whereas in this paper, we favor a symbol-rate beamforming at the base station. The new approach optimizes the actual values of the decision variables of the rake demodulators at the receivers. The superiority of the symbol rate beamforming algorithm compared to slotwise beamforming will be shown by bit error rate (BER) simulations.**

***Index Terms*—Beamforming, downlink processing, DS-CDMA, interference suppression, symbol rate.**

I. Introduction

DIRECT-SEQUENCE (DS) code division multiple access (CDMA) will be a major part of the third–generation (3G) systems. In January 1998, the *European Telecommunications Standards Institute* (ETSI) agreed to base the *frequency division duplex* (FDD) transmission on *wideband* CDMA (WCDMA), which is examined in this article as an example of DS-CDMA. In the FDD mode, the different stations transmit simultaneously, and the different transmissions are distinguished by *spreading codes*, which change over time due to scrambling. To regain the transmitted data values at the receiving station, the received signal has to be correlated with the respective spreading code. Consequently, we review the correlation properties of the utilized spreading codes in Section III. The uplink has already been investigated extensively, e.g., in [6] and [7], in contrast to the downlink, where only few contributions exist, e.g., [8], although in future services of 3G mobile radio communication, the data rates in the downlink will be higher than in the uplink. Thus, we only concentrate on the downlink. Due to economic considerations, we assume that the *base station* (BS) is equipped with an antenna array, whereas the *mobile stations* (MS) have only one antenna and a conventional maximum ratio combining rake demodulator. Therefore, space–time processing is only possible during sending but impossible during receiving. Consequently, we develop a *beamforming* algorithm for the BS. After explaining the system model and discussing the reciprocity of the channel parameters of the uplink and the downlink in Section II, we focus on the code correlation properties in Section III. Section IV contains an approach to define the rake finger weights at the receiver. In Section V, we present a symbol rate downlink beamforming algorithm, i.e., the beamforming vectors change from symbol to symbol. Section VI gives a brief summary of the proposed downlink beamforming algorithm, and Section VII presents bit error rate (BER) simulation results.

Manuscript received August 1, 1999; revised June 1, 2000. This paper was presented in part at the 10th International Symposium on Personal, Indoor, and Mobile Radio Communications, Osaka, Japan, September 12–15, 1999.

The authors are with the Institute for Circuit Theory and Signal Processing, Munich University of Technology, Munich, Germany (e-mail: mijo@nws.ei.tum.de; wout@nws.ei.tum.de).

Publisher Item Identifier S 0733-8716(01)00957-X.

II. System Model

A. DS-CDMA Modulation

We examine WCDMA, which is a DS-CDMA system [9], [10]. The mth symbol $s_k^{(m)} \in \{-1, +1\}$ (in the case of BPSK modulation) of user $k \in \{1, \ldots, K\}$ is spread by a spreading code $c_k^{(m)}[l]$, which is composed of the *orthogonal variable spreading factor* (OVSF) [11] code $o_k[l]$ and the pseudo-noise scrambling code $g[l]$ of length SF_k and N_g, respectively

$$c_k^{(m)}[l] = o_k[l]\, g\left[(mSF_k + l) \bmod N_g\right]. \tag{1}$$

Here "mod" denotes modulo division. After pulse shaping, the resulting baseband DS-CDMA signal dedicated to MS k reads as

$$s_k(t) = \sum_{m=-\infty}^{\infty} s_k^{(m)} \sum_{l=0}^{SF_k-1} c_k^{(m)}[l]\, p_{\mathrm{rc}}\left(t - (l + mSF_k)T_c\right) \tag{2}$$

where $p_{\mathrm{rc}}(t)$ and T_c are the Nyquist chip waveform, which is a raised cosine with rolloff $\alpha = 0.22$ in the frequency domain [12] and the chip duration, respectively. Note that we moved the matched filtering of the MSs to the BS for notational simplicity. Thus, the root-raised cosine impulse used in WCDMA becomes a raised cosine impulse.

B. Channel Model

At the BS, the signals $s_k(t)$ dedicated to the different MS are weighted, added, and then sent via the antenna array. Therefore, every MS receives portions of all sent signals $s_{k'}(t)$

$$r_k(t) = \sum_{k'=1}^{K} h_k^{(k',m)}(t) * s_{k'}(t) + n_k(t). \tag{3}$$

Here "$*$," K, and $n_k(t)$ denote linear convolution, the number of MSs, and *intercell interference* combined with *noise* at MS k, which are both assumed to be white Gaussian random processes, respectively.

The BS has estimated the channel parameters in the uplink. Each of the Q discrete paths leading to MS k is represented by the steering vector $\boldsymbol{a}_{k,q} \in \mathbb{C}^M$, where M is the number of antenna elements at the BS, the transmission factor $p_{k,q} \in \mathbb{R}$ (the reciprocal of the respective path attenuation), the path-delay time $\tau_{k,q}$, and the path-phase shift $\varphi_{k,q}$ [13]. As a consequence, the channel impulse response representing the transmission of $s_{k'}(t)$ to MS k for the mth symbol expressed with the parameters of the multipaths can be written as

$$h_k^{(k',m)}(t) = \sum_{q=1}^{Q} p_{k,q} \boldsymbol{a}_{k,q}^{\mathrm{T}} \boldsymbol{w}_{k'}^{(m)} e^{\mathrm{j}\varphi_{k,q}} \delta(t - \tau_{k,q}). \quad (4)$$

Note that the channel impulse responses $h_k^{(k',m)}(t)$, $k' = 1, \ldots, K$, representing the transmission to MS k only differ in the *beamforming vector* $\boldsymbol{w}_{k'}^{(m)}$, which changes from symbol to symbol, and therefore, the $h_k^{(k',m)}(t)$ change symbolwise.

C. Reciprocity of the Channel Parameters

Our downlink beamforming algorithm is based on the channel parameters estimated in the uplink. For the estimation, a channel-sounding algorithm is needed, e.g., the one presented in [2]. In WCDMA, the uplink frequency band resides 190 MHz higher than the downlink frequency band [9]. Therefore, not every channel parameter estimated in the uplink can be used directly in the downlink. We assume that the frequency gap is small enough so that the directions of arrival (DOAs) represented by azimuth and elevation are the same for both frequencies [14]. Consequently, the steering vector estimated in the uplink just has to be transformed with regard to the different frequency in the downlink [15]. We also presume that the directions change very slowly. Therefore, the coherence time of the DOAs is noticeably larger than the duration of one slot. Both assumptions, that the frequency gap is small enough and the coherence time is large enough, justify the usage of the DOAs estimated in the uplink for downlink transmission. Because the DOAs are the same for both links, the path delays must also be the same since the delay is the division of the path length by the speed of light. Moreover, the path delays change very slowly over time due to the dependence on the DOAs.

The only channel parameter which can be estimated in the uplink that is not fully reciprocal is the complex amplitude. First, the frequency offset between uplink and downlink results in completely different phase shifts of each path. Second, the amplitude changes due to fast fading. However, we propose that the medium-term average transmission factor is the same for the uplink and the downlink, since it depends on the DOA. Additionally, we assume that the medium-term average transmission factor varies slowly like the DOA and the path delay do. Only the path phase shift is unknown. Unfortunately, the symbol rate downlink-beamforming algorithm (cf. Section V) needs the values of the path phase shifts in order to perform a coherent superposition of the different signal portions received by the MSs. Therefore, we propose a feedback of the unknown phases from the MSs to the BS.

D. Feedback from the Mobile Stations to the Base Station

All parameters except the path phase shifts $\varphi_{k,q}$ in (4) are known to the BS. To be able to compute the demanded beamforming vectors $\boldsymbol{w}_{k'}^{(m')}$, we need the knowledge of the path phase shifts, too. Our solution to remove this lack of knowledge is a feedback of the unknown phase shifts from the MSs to the BS. In [16], Gerlach and Paulraj also proposed a feedback from the MSs to the BS, but their approach was designed for the *advanced mobile phone system* (AMPS). This analog system has negligible delay spread. Therefore, one steering vector is sufficient to describe the transmission to the respective MS. In a multipath system, however, an ensemble of vectors has to be transmitted from every MS to the BS, leading to a high feedback data rate. We propose another feedback. The BS only needs to know the difference of the unknown phase shifts of the different paths since the other channel parameters can be estimated in the uplink. The feedback does not decrease the system performance because the demanded data rates will be much higher in the downlink than in the uplink. Therefore, the saved capacity of the uplink mode can be used for the feedback of the phase information. We do not concentrate on the feedback itself in this paper. Future research will show how many bits have to be used for each phase value and how the performance of the downlink transmission depends on the accuracy of the phase values.

III. Code Correlation Properties

To give a motivation for symbolwise beamforming, we review the properties of the scrambled spreading codes $c_k^{(m)}[l]$. We presume conventional maximum ratio-combining rake receivers at the MSs. The output stage of a rake demodulator includes an integrate-and-dump unit. Hence, we have to examine a "windowed" correlation function of the codes dedicated to MS k and k'

$$\mathrm{CCF}_{k,k'}^{(m)}[n] = \sum_{l=0}^{SF-1} c_k^{(m)}[l] c_{k'}^{(m)}[l+n]. \quad (5)$$

Note that we have chosen the same spreading factor SF for both codes since we can split the codes into partitions of the same length as follows from the generation process of OVSF codes [11].

Due to scrambling, the code correlation properties change from symbol to symbol, as can be seen for autocorrelation and crosscorrelation in Figs. 1 and 2, respectively. The scrambling does not only effect the instantaneous correlation properties. It also improves the mean correlation properties, which are the correlation functions averaged over the maximum number of symbols in a slot. This property is exploited for the predefinition of the rake finger weights, cf. Section IV.

IV. Predefinition of the Rake Finger Weights

The predefinition of the rake finger weights is performed during the transmission of the pilot symbols. The idea is to transmit the pilot symbols with *constant* beamforming vectors

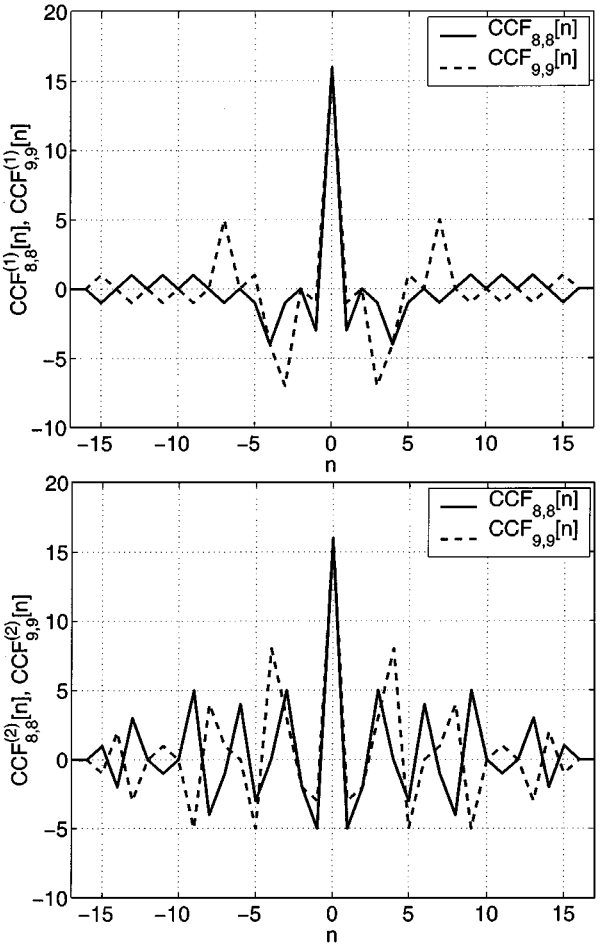

Fig. 1. Autocorrelation properties of the scrambled OVSF codes 8 and 9 with $SF = 16$.

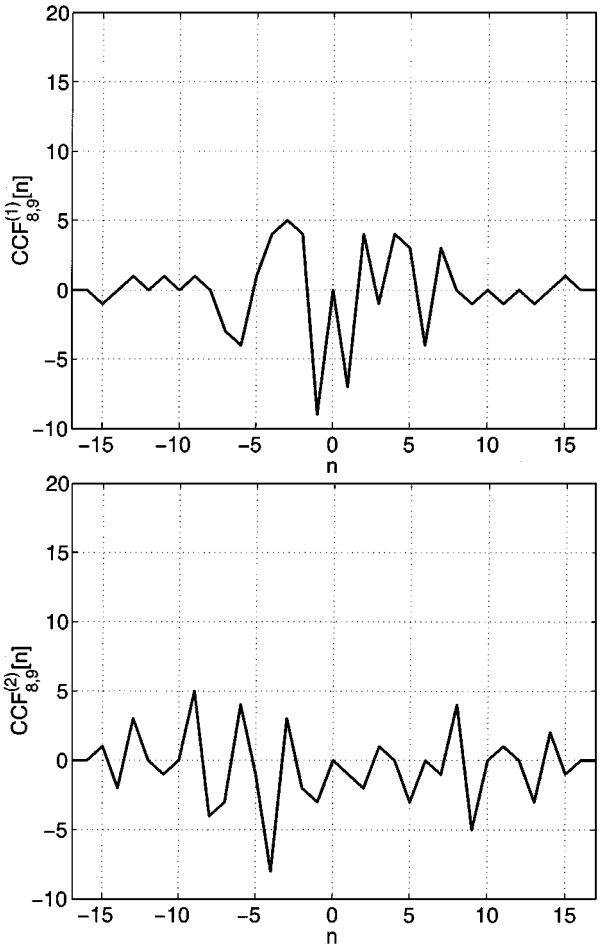

Fig. 2. Crosscorrelation properties of the scrambled OVSF codes 8 and 9 with $SF = 16$.

$\boldsymbol{w}_k^{\text{pilot}}$. Then, the rake receiver "learns" the intended rake finger weights during the channel estimation process when receiving the pilot symbols.

The rake demodulator exploits the pilot symbols at the beginning of each slot to estimate the channel impulse response $h_k^{(k)}(t)$. Note that we dropped the index m in this section because the channel impulse response is constant during the transmission of the pilot symbols. The rake demodulator correlates with the N_p pilot symbols and gets a channel estimation for each pilot symbol. The overall channel estimation is the mean of the estimations made with each pilot symbol. The averaging of the channel estimations is equal to an averaging of the correlation properties of the spreading codes. As stated in Section III, the mean correlation properties are approximately ideal. Thus, the averaging leads to a decoupling of signals dedicated to the different MSs. As a consequence, we need not regard the signals of the other MSs. Moreover, the interference caused by the signal itself due to the autocorrelation function can be neglected also.

The rake finger weights which are the complex conjugate of the respective channel taps can be written as

$$v_{k,f} = \left(h_{k,f}^{(k)}\right)^* = p_{k,f}\left(\boldsymbol{w}_k^{\text{pilot}}\right)^{\text{H}} \boldsymbol{a}_{k,f}^* e^{-\text{j}\varphi_{k,f}}. \quad (6)$$

As stated above, we do not have to consider the signal portions caused by *co-channel interference* (CCI) and *intersymbol interference* (ISI) since the mean correlation properties of the spreading codes are approximately ideal due to scrambling. We propose to maximize the transmission power of the channel impulse response taps $h_{k,f}^{(k)}$ belonging to the F strongest paths connecting the BS and MS k, where F is the number of rake fingers. The power of one tap reads as

$$P_{k,f} = \left(h_{k,f}^{(k)}\right)^* h_{k,f}^{(k)} = \left(\boldsymbol{w}_k^{\text{pilot}}\right)^{\text{H}} \boldsymbol{a}_{k,f}^* p_{k,f}^2 \boldsymbol{a}_{k,f}^{\text{T}} \boldsymbol{w}_k^{\text{pilot}}. \quad (7)$$

Additionally, we can choose the same transmission power for all pilot signals because interference is cancelled due to the approximately ideal correlation properties. This leads to following optimization problem

$$\max_{\boldsymbol{w}_k^{\text{pilot}}} \sum_{f=1}^{F} P_{k,f} = \max_{\boldsymbol{w}_k^{\text{pilot}}} \left(\boldsymbol{w}_k^{\text{pilot}}\right)^{\text{H}} \boldsymbol{A}_k^* \boldsymbol{A}_k^{\text{T}} \boldsymbol{w}_k^{\text{pilot}}$$
$$\text{s. t.:} \left(\boldsymbol{w}_k^{\text{pilot}}\right)^{\text{H}} \boldsymbol{w}_k^{\text{pilot}} = 1 \quad (8)$$

where

$$\boldsymbol{A}_k = [p_{k,1}\boldsymbol{a}_{k,1}, \ldots, p_{k,F}\boldsymbol{a}_{k,F}] \in \mathbb{C}^{M \times F} \quad (9)$$

is the steering matrix containing the steering vectors $\boldsymbol{a}_{k,f}$ weighted with the respective transmission factor $p_{k,f}$. The solution of the optimization problem in (8) is the eigenvector

belonging to the largest eigenvalue of $\boldsymbol{A}_k^* \boldsymbol{A}_k^{\mathrm{T}}$. The BS is then able to compute the rake finger weights $v_{k,f}$ by using (6).

V. Symbol Rate Downlink Beamforming

The BS is equipped with an array of M antennas. Therefore, it is able to perform beamforming. We exploit the additional spatial degrees of freedom to reduce the deficiency of the spreading codes to separate the different users. Because the codes change from symbol to symbol, we present a symbolwise beamforming algorithm. The rake demodulator estimates the F strongest channel impulse response taps exploiting the pilot symbols at the beginning of each slot and sets the rake finger weights $v_{k,f}$ to the conjugate complex of the respective channel impulse response tap. We presume a utilization of the rake finger predefinition algorithm presented in Section IV. Thus, the BS knows the rake finger weights $v_{k,f}$. The maximum ratio combining rake receiver samples the received signal $r_k(t)$, cf. (3), at OSF times the chip rate $1/T_c$, correlates the obtained $r_k[l]$ with the spreading code $c_k^{(m)}[l]$, and performs maximum ratio combining. Thus, the detection signal for the mth symbol of the rake demodulator at MS k can be expressed as

$$u_k^{(m)} = \mathrm{Re}\left\{ \sum_{f=1}^{F} v_{k,f} \sum_{l=0}^{SF_k-1} c_k^{(m)}[l] r_k[OSFl + l_{k,f}] \right\} \quad (10)$$

where we introduced the discrete time delay $l_{k,f} = \tau_{k,f} OSF/T_c$. After defining the correlation function

$$\begin{aligned} \mathrm{CCF}_{k,k'}^{(m,m')}[n] = & \sum_{l=0}^{SF} c_k^{(m)}[l] \sum_{l'=0}^{SF} c_{k'}^{(m')}[l'] \\ & \cdot p_{rc}[OSF(l-l'+(m-m')SF+n)] \end{aligned} \quad (11)$$

between the spreading codes of MSs k and k' and symbols m and m' which regards the raised cosine impulse form sampled at OSF times the chip rate, inserting (4), and neglecting noise and intercell interference, the rake demodulator output can be written as

$$\begin{aligned} u_k^{(m)} = \mathrm{Re}\Bigg\{ & \sum_{f=1}^{F} v_{k,f} \sum_{k'=1}^{K} \sum_{m'=-\infty}^{\infty} \sum_{q=1}^{Q} p_{k,q} \boldsymbol{a}_{k,q}^{\mathrm{T}} e^{\mathrm{j}\varphi_{k,q}} \\ & \cdot \boldsymbol{w}_{k'}^{(m)} s_{k'}^{(m')} \mathrm{CCF}_{k,k'}^{(m,m')}[l_{k,f} - l_{k,q}] \Bigg\}. \end{aligned} \quad (12)$$

We assume that the delay spread is small ($\tau_{\max} < T_k$). Thus, we can drop the sum over m' because the ISI is negligible. Hence, we end up with

$$\begin{aligned} u_k^{(m)} = \mathrm{Re}\Bigg\{ & \sum_{f=1}^{F} \sum_{k'=1}^{K} \sum_{q=1}^{Q} v_{k,f} p_{k,q} \boldsymbol{a}_{k,q}^{\mathrm{H}} e^{\mathrm{j}\varphi_{k,q}} \\ & \cdot \boldsymbol{w}_{k'}^{(m)} s_{k'}^{(m)} \mathrm{CCF}_{k,k'}^{(m,m)}[l_{k,f} - l_{k,q}] \Bigg\}. \end{aligned} \quad (13)$$

A. Compact Reformulation of the Rake Output Signal

It is convenient to combine the variables belonging to a particular path q in the vector

$$\boldsymbol{b}_{k,q} = p_{k,q} \boldsymbol{a}_{k,q}^* e^{-\mathrm{j}\varphi_{k,q}} \in \mathbb{C}^M \quad (14)$$

and the signals of symbol m at the BS in the vector

$$\boldsymbol{z}_{k'}^{(m)} = s_{k'}^{(m)} \boldsymbol{w}_{k'}^{(m)} \in \mathbb{C}^M. \quad (15)$$

Substituting these abbreviations into (13), the rake demodulator output signal can be expressed as follows:

$$\begin{aligned} u_k^{(m)} = \mathrm{Re}\Bigg\{ & \sum_{f=1}^{F} \sum_{k'=1}^{K} \sum_{q=1}^{Q} v_{k,f} \boldsymbol{b}_{k,q}^{\mathrm{H}} \boldsymbol{z}_{k'}^{(m)} \\ & \cdot \mathrm{CCF}_{k,k'}^{(m,m)}[l_{k,f} - l_{k,q}] \Bigg\}. \end{aligned} \quad (16)$$

Note that $\boldsymbol{b}_{k,q}$ and $v_{k,q}$ are constant, and only the correlation function $\mathrm{CCF}_{k,k'}^{(m,m)}[n]$ changes from symbol to symbol. With the definition of

$$\boldsymbol{z}^{(m)} = \left[\boldsymbol{z}_1^{(m),\mathrm{T}}, \cdots, \boldsymbol{z}_K^{(m),\mathrm{T}} \right]^{\mathrm{T}} \in \mathbb{C}^{MK} \quad (17)$$

and the $\mathbb{C}^{MK}$ vector

$$\begin{aligned} \boldsymbol{g}_{k,f,q}^{(m)} = \Big[& \mathrm{CCF}_{k,1}^{(m,m)}[l_{k,f} - l_{k,q}], \cdots \\ & \mathrm{CCF}_{k,K}^{(m,m)}[l_{k,f} - l_{k,q}] \Big]^T \otimes (v_{k,f}^* \boldsymbol{b}_{k,q}) \end{aligned} \quad (18)$$

where "$\otimes$" denotes the Kronecker product, and moving the double sum into the vector

$$\boldsymbol{g}_k^{(m)} = \sum_{q=1}^{Q} \sum_{f=1}^{F} \boldsymbol{g}_{k,f,q}^{(m)} \in \mathbb{C}^{MK} \quad (19)$$

we get the compact reformulation of (17), which is a simple dot product

$$u_k^{(m)} = \mathrm{Re}\left\{ \boldsymbol{g}_k^{(m),\mathrm{H}} \boldsymbol{z}^{(m)} \right\}. \quad (20)$$

If a modulation scheme different of BPSK (e.g., QPSK) is used, only the $\mathrm{Re}\{\bullet\}$ operator has to be dropped. Again, note that the only changing parts in the representation of $u_k^{(m)}$ are the correlation functions which influence $\boldsymbol{g}_k^{(m)}$. We only have to compute the correlation functions, the Kronecker products, and the double sum for each symbol.

B. Transformation to a Real-Valued Representation of the Rake Output Signal

Because we assume BPSK modulation, a transformation to a real-valued representation of the rake detection signal is advantageous. Therefore, we stack the real part and the imaginary

part of the two vectors $\boldsymbol{z}^{(m)}$ and $\boldsymbol{g}_k^{(m)}$ onto each other and get the $\mathbb{R}^{2MK}$ vectors

$$\boldsymbol{x}^{(m)} = \left[\mathrm{Re}\left\{\boldsymbol{z}^{(m)}\right\}^{\mathrm{T}}, \mathrm{Im}\left\{\boldsymbol{z}^{(m)}\right\}^{\mathrm{T}}\right]^{\mathrm{T}} \tag{21}$$

$$\boldsymbol{\gamma}_k^{(m)} = \left[\mathrm{Re}\left\{\boldsymbol{g}_k^{(m)}\right\}^{\mathrm{T}}, \mathrm{Im}\left\{\boldsymbol{g}_k^{(m)}\right\}^{\mathrm{T}}\right]^{\mathrm{T}}. \tag{22}$$

We end up with a real-valued representation of the rake demodulator output signal for the mth symbol:

$$u_k^{(m)} = \boldsymbol{\gamma}_k^{(m),\,\mathrm{T}} \boldsymbol{x}^{(m)}. \tag{23}$$

C. Development of the Symbol Rate Downlink Beamforming Algorithm

Our goal is to provide the demanded level for the decision signal of every rake receiver. In other words, we have to fulfill K requirements

$$u_k^{(m)} = s_k^{(m)} \theta_k, \qquad k = 1, \ldots, K \tag{24}$$

where $\theta_k \in \mathbb{R}_+$ is a parameter, which depends on the signal level that is demanded by MS k. If a MS is in a noisy environment (e.g., near cell border), the respective θ_k can be increased, leading to a higher signal level at the MSs output. Therefore, fast *transmit power control* (TPC) can be easily implemented. If MS k demands a larger or smaller receive power, the parameter θ_k just has to be increased or decreased, respectively. Note that we do not optimize the SNR at the receiver directly. However, if MS k receives high (low) noise power, its TPC commands will lead to a larger (smaller) θ_k, and consequently, MS k will receive more (less) signal power. Hence, the SNR at the receiver is optimized indirectly. The requirements in (24) can be seen as zero-forcing constraints because the noise process is disregarded. However, due to the update of θ_k depending on TPC commands, the disadvantage of zero-forcing solutions is removed since the MS demands a larger or smaller reception power depending on the actual impact of the noise process.

Since the beamforming vectors are computed symbolwise, the number of degrees of freedom per symbol is $2MK$. On the other hand, we must fulfill K constraints, cf. (24). Hence, the number of degrees of freedom is larger than the number of restrictions. We exploit the remaining degrees of freedom to reduce the transmit power at the BS. This leads to following optimization problem for BPSK:

$$\min_{\boldsymbol{x}^{(m)}} \left\|\boldsymbol{x}^{(m)}\right\|_2^2 \quad \text{s. t.: } \boldsymbol{\Gamma}^{(m)} \boldsymbol{x}^{(m)} = \boldsymbol{\theta} \tag{25}$$

where

$$\boldsymbol{\Gamma}^{(m)} = \left[s_1^{(m)} \boldsymbol{\gamma}_1^{(m)}, \ldots, s_K^{(m)} \boldsymbol{\gamma}_K^{(m)}\right]^{\mathrm{T}} \in \mathbb{R}^{K \times 2MK} \tag{26}$$

and

$$\boldsymbol{\theta} = [\theta_1, \ldots, \theta_K]^{\mathrm{T}} \in \mathbb{R}_+^K. \tag{27}$$

TABLE I
BERs FOR LOOK-DIRECTION SLOT-WISE AND SYMBOL-WISE JOINT DOWNLINK BEAMFORMING

MS	BER – slot	BER – symbol
1	$1.95 \cdot 10^{-2}$	$3.35 \cdot 10^{-3}$
2	$0.43 \cdot 10^{-2}$	$2.49 \cdot 10^{-3}$
3	$8.63 \cdot 10^{-2}$	$0.41 \cdot 10^{-3}$
4	$4.88 \cdot 10^{-2}$	$10 \cdot 10^{-3}$
5	$0.14 \cdot 10^{-2}$	$0.05 \cdot 10^{-3}$
6	$1.62 \cdot 10^{-2}$	$5.57 \cdot 10^{-3}$
7	$0.92 \cdot 10^{-2}$	$0.19 \cdot 10^{-3}$
8	$0.66 \cdot 10^{-2}$	$1.06 \cdot 10^{-3}$
9	$0.15 \cdot 10^{-2}$	$4.01 \cdot 10^{-3}$
10	$1.20 \cdot 10^{-2}$	$6.60 \cdot 10^{-3}$
11	0	0
12	$0.01 \cdot 10^{-2}$	0
13	0	0
14	0	0

TABLE II
MEAN BERs FOR LOOK-DIRECTION SLOT-WISE AND SYMBOL-WISE JOINT DOWNLINK BEAMFORMING

	mean BER
slot-wise	$1.47 \cdot 10^{-2}$
symbol-wise	$1.70 \cdot 10^{-3}$

Note that the rows of $\boldsymbol{\Gamma}^{(m)}$ in (26) are weighted with the symbol values $s_k^{(m)}$ to move $s_k^{(m)}$ to the left side of (24). Thus, the result of the multiplication $\boldsymbol{\Gamma}^{(m)} \boldsymbol{x}^{(m)}$ must be the vector $\boldsymbol{\theta}$ containing positive real-valued numbers. Again, the parameter $\theta_k \in \mathbb{R}_+$ in (27) is the absolute value of the demanded decision signal of the rake demodulator k and adjusts the robustness of decision of the kth detector. For QPSK, a transformation to a real-valued representation is not necessary, and the resulting optimization reads as

$$\min_{\boldsymbol{z}^{(m)}} \left\|\boldsymbol{z}^{(m)}\right\|_2^2, \qquad \text{s. t.: } \boldsymbol{G}^{(m)} \boldsymbol{z}^{(m)} = \boldsymbol{\theta} \tag{28}$$

with

$$\boldsymbol{G}^{(m)} = \left[s_1^{(m)} \boldsymbol{g}_1^{(m)}, \ldots, s_K^{(m)} \boldsymbol{g}_K^{(m)}\right]^{\mathrm{H}} \in \mathbb{C}^{K \times MK}. \tag{29}$$

Every row of $\boldsymbol{G}^{(m)}$ is weighted with the conjugate complex of the symbol values $s_k^{(m),\,*}$.

The solution of the optimization problem in (25) can be easily obtained, e.g., by introducing Lagrange multipliers, and can be written as

$$\boldsymbol{x}^{(m)} = \boldsymbol{\Gamma}^{(m),\,\mathrm{T}} \left(\boldsymbol{\Gamma}^{(m)} \boldsymbol{\Gamma}^{(m),\,\mathrm{T}}\right)^{-1} \boldsymbol{\theta}. \tag{30}$$

The wanted beamforming vector $\boldsymbol{w}_k^{(m)}$ is the multiplication of $\boldsymbol{z}_k^{(m)}$ with the symbol $s_k^{(m)}$ to solve (15), where $\boldsymbol{z}_k^{(m)}$ is the complex vector, whose real and imaginary parts are the first and the second half of $\boldsymbol{x}^{(m)}$, cf. (21). For QPSK, the result is the multiplication with the pseudo-inverse of $\boldsymbol{G}^{(m)}$:

$$\boldsymbol{z}^{(m)} = \boldsymbol{G}^{(m),\,\dagger} = \boldsymbol{G}^{(m),\,\mathrm{H}} \left(\boldsymbol{G}^{(m)} \boldsymbol{G}^{(m),\,\mathrm{H}}\right)^{-1} \boldsymbol{\theta} \tag{31}$$

and we have to multiply $\boldsymbol{z}_k^{(m)}$ with the complex conjugate of the symbol $s_k^{(m),*}$ to obtain $\boldsymbol{w}_k^{(m)}$.

VI. Brief Summary of the Proposed Downlink Beamforming Algorithm

previous uplink slot :
estimate (or update the estimate) of the channel parameters: steering vector $\boldsymbol{a}_{k,q}$, path delay $\tau_{k,q}$ (discrete time: $l_{k,q}$), medium-term average transmission factor $p_{k,q}$
receive the update of the path phase shift $\varphi_{k,q}$
compute the new $\boldsymbol{b}_{k,q}$ (cf. 14)
compute the beamforming vectors $\boldsymbol{w}_k^{\text{pilot}}$ for the pilot sequence as the principal eigenvector of $\boldsymbol{A}_k^*\boldsymbol{A}_k^{\text{T}}$ (cf. 9)
calculate the rake finger weights $v_{k,f}$ with Equation (6)
update θ_k depending on TPC commands

pilot phase :
transmit the pilot sequences with the previously computed beamforming vectors $\boldsymbol{w}_k^{\text{pilot}}$

transmission of data symbol m **:**
compute the correlation functions $\text{CCF}_{k,k'}^{(m,m)}[l_{k,f} - l_{k,q}]$
evaluate (18) and (19) to get $\boldsymbol{g}_k^{(m)}$
transform to real-valued $\boldsymbol{\gamma}_k^{(m)}$ with (22)
calculate $\boldsymbol{x}^{(m)}$ (cf. 30)
real part and imaginary part of $\boldsymbol{z}^{(m)}$ are the first and second half of $\boldsymbol{x}^{(m)}$, respectively
split $\boldsymbol{z}^{(m)}$ into K pieces $\boldsymbol{z}_k^{(m)}$ (cf. 17)
compute the beamforming vector $\boldsymbol{w}_k^{(m)}$ with (15)
transmit the symbol $s_k^{(m)}$ spread with $c_k^{(m)}[l]$ and weighted with the beamforming vector $\boldsymbol{w}_k^{(m)}$

VII. Simulation Results

We compare our new symbol rate downlink beamforming algorithm to the look-direction beamforming approach. This slotwise approach sets the beamforming vectors equal to the steering vector of the strongest path leading to the respective MS. We try to minimize the number of necessary antenna elements at the BS. We chose $M = 3$ antennas. Our simulation scenario includes $K = 14$ MSs, where $Q = 7$ paths connect each MS with the BS, cf. Table III. The directions of arrival $\boldsymbol{a}_{k,q}$ and the transmission factors $p_{k,q}$, $k = 1, \ldots, K$ and $q = 1, \ldots, Q$ are constant. The path phase shifts $\varphi_{k,q}$ and the delay times $\tau_{k,q}$ are uniformly distributed within the intervals $[0, 2\pi]$ and $[-\tau_{\max}, +\tau_{\max}]$, respectively. The delay spread $\tau_{\max}$ is 2 μs, which is about the half of a symbol time for the used spreading factor $SF = 16$. The rake receiver oversamples with $OSF = 4$ and has $F = 3$ fingers.

TABLE III
Simulation Scenario

k	q	$\theta_{k,q}$	$p_{k,q}$	k	q	$\theta_{k,q}$	$p_{k,q}$
	1	0°	1		1	310°	1
	2	345°	0.95		2	305°	0.95
	3	20°	0.9		3	343°	0.72
1	4	40°	0.8	8	4	313°	0.57
	5	330°	0.7		5	299°	0.55
	6	320°	0.5		6	290°	0.1
	7	50°	0.3		7	1°	0.09
	1	45°	1		1	333°	1
	2	60°	0.9		2	338°	0.98
	3	35°	0.85		3	328°	0.9
2	4	5°	0.6	9	4	358°	0.8
	5	340°	0.5		5	308°	0.5
	6	70°	0.2		6	305°	0.2
	7	−40°	0.1		7	325°	0.1
	1	30°	1		1	70°	1
	2	343°	0.88		2	65°	0.91
	3	320°	0.8		3	72°	0.82
3	4	20°	0.7	10	4	33°	0.73
	5	355°	0.55		5	49°	0.64
	6	13°	0.3		6	62°	0.55
	7	40°	0.05		7	30°	0.46
	1	315°	1		1	238°	1
	2	7°	0.88		2	156°	0.485
	3	39°	0.75		3	175°	0.065
4	4	352°	0.66	11	4	241°	0.017
	5	333°	0.6		5	165°	0.005
	6	75°	0.2		6	175°	0.004
	7	−43°	0.09		7	244°	0.003
	1	5°	1		1	185°	1
	2	355°	0.6		2	165°	0.37
	3	10°	0.5		3	185°	0.3
5	4	15°	0.4	12	4	181°	0.108
	5	330°	0.2		5	189°	0.075
	6	335°	0.05		6	185°	0.061
	7	20°	0.01		7	177°	0.057
	1	10°	1		1	59°	1
	2	13°	0.8		2	59°	0.262
	3	8°	0.75		3	63°	0.076
6	4	17°	0.7	13	4	288°	0.037
	5	21°	0.65		5	18°	0.036
	6	3°	0.6		6	14°	0.029
	7	348°	0.5		7	76°	0.023
	1	37°	1		1	14°	1
	2	42°	0.71		2	9°	0.034
	3	349°	0.61		3	18°	0.0277
7	4	32°	0.59	14	4	5°	0.008
	5	47°	0.585		5	0°	0.003
	6	336°	0.4		6	355°	0.002
	7	70°	0.35		7	350°	0.001

The transmission power $\sum \|\boldsymbol{w}_k\|_2^2$ is set to $1 \hat{=} 0$ dB and is the same for both the slotwise and symbolwise beamforming. Also, the additive white Gaussian noise (AWGN), which models the intercell interference and noise, is the same for all MSs and both

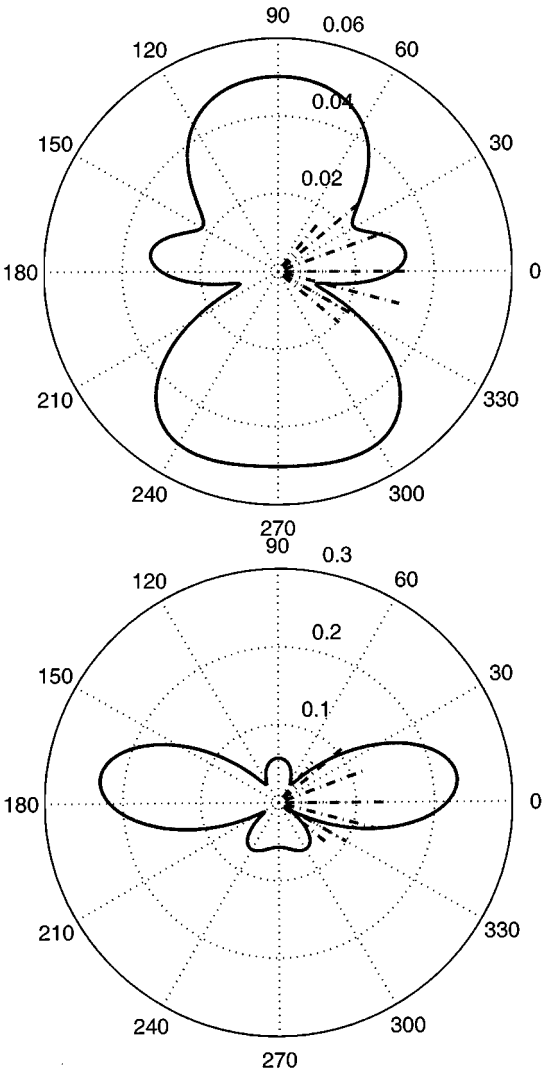

Fig. 3. Beam pattern for the symbolwise beamforming algorithm: solid lines; paths: dashdotted lines.

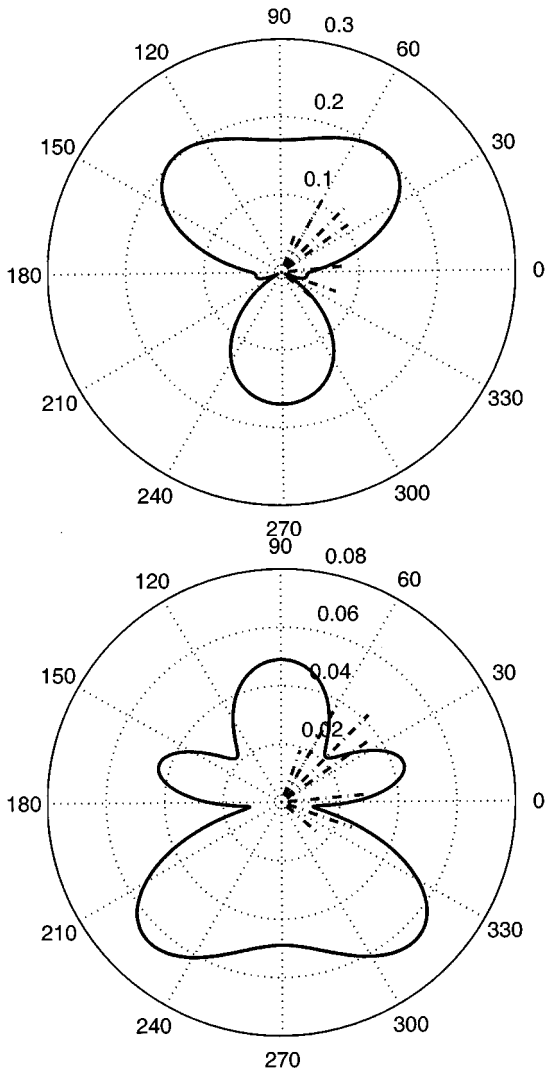

Fig. 4. Beam pattern for the symbolwise beamforming algorithm: solid lines; paths: dashdotted lines.

beamforming methods, and we chose a value of -10 dB with respect to the transmission power.

Each slot consists of 2560 symbols or 40 960 chips, which is equal to the length of the used Gold scrambling sequence. Note that in the new version of standardization [17], [18], the length of the Gold sequence is $N_g = 38\,400$. The results shown in Tables I and II are the mean of 150 simulations. We observe a significant improvement of the BER with the symbolwise beamforming compared to the slotwise look-direction method. However, the BER for MS 9 is higher for symbolwise beamforming than for slotwise beamforming. The explanation can be found in the very large transmission factors $p_{9,q}$ of MS 9, cf. Table III. In the development of the symbolwise downlink beamforming algorithm, we made the assumption that the delay spread $\tau_{\max}$ is small enough so that we can neglect the signal portions due to the previously and afterwards transmitted symbols. This assumption holds as long as the transmission factors of the weaker paths are small enough. In the case of MS 9, the weaker paths are very strong (0.98, 0.9, 0.8, 0.5). Therefore, the probability that the assumption does not hold is higher than for other MSs, e.g., MS 5 (0.6, 0.5, 0.4, 0.2).

The beampattern computed by the symbolwise downlink-beamforming algorithm changes completely from symbol to symbol, as can be seen in Figs. 3 and 4. The beampattern changes substantially and cannot be explained with the directions of the different MSs because the algorithm also considers the code correlation properties, which change from symbol to symbol and, moreover, takes into account the values of the data symbols, which have to be transmitted.

We also present the averaged beampattern of the symbolwise downlink-beamforming algorithm in Fig. 5. The average beampattern (averaged over 100 symbols) is nearly the same as for the look-direction beamforming approach. Therefore, we find again a motivation to compare the symbolwise beamforming algorithm to the look-direction method, because the look-direction method leads to beamforming vectors, which are similar to the averaged symbolwise beamforming vectors.

VIII. Conclusion

We have presented a new downlink beamforming algorithm for DS-CDMA systems, which computes the beamforming weights symbolwise. The symbol rate computation of the

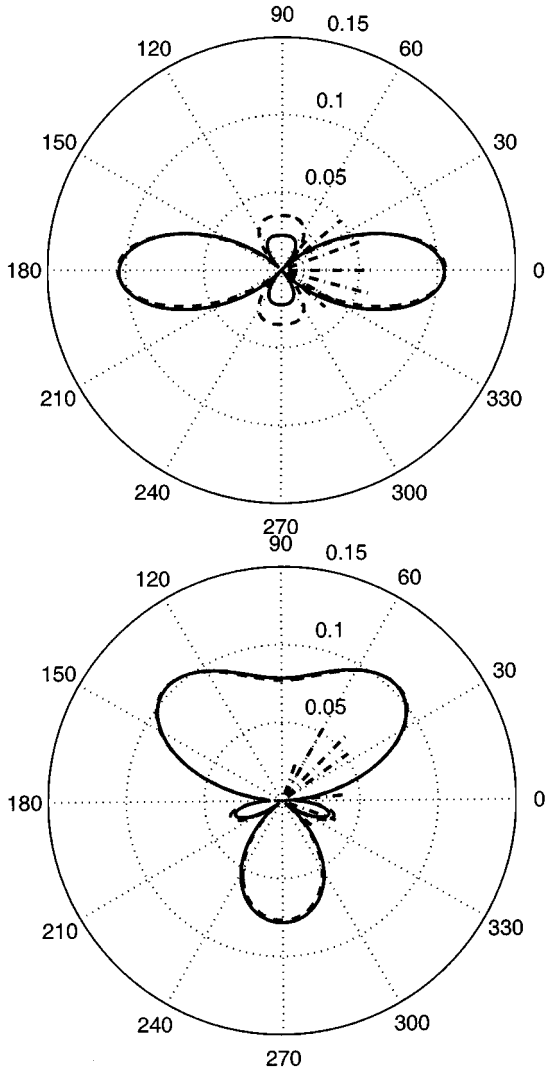

Fig. 5. Average beam pattern for the symbol-wise beamforming algorithm: solid lines; look-direction: dashed lines; paths: dashdotted lines.

beamforming vectors has been motivated by the change of correlation properties of the scrambled spreading sequences, and the algorithm was developed to provide the demanded signal level at the demodulator output of the respective MS. The simulation results show the superiority of symbolwise processing over slotwise processing.

REFERENCES

[1] A. F. Naguib, A. Paulraj, and T. Kailath, "Performance of CDMA cellular networks with base-station antenna arrays: The downlink," in *Proc. ICC*, vol. 2, May 1994, pp. 795–799.

[2] M. Haardt, C. Brunner, and J. A. Nossek, "Efficient high-resolution 3-D channel sounding," in *Proc. Veh. Technol. Conf.*, vol. 1, May 1998, pp. 164–168.

[3] E. H. Dinan and B. Jabbari, "Spreading codes for direct sequence CDMA cellular networks," *IEEE Commun. Mag.*, vol. 36, pp. 48–54, Sept. 1998.

[4] C. Brunner, M. Joham, W. Utschick, M. Haardt, and J. A. Nossek, "Downlink beamforming for WCDMA based on uplink channel parameters," in *Proc. EPMCC*, Mar. 1999, pp. 375–380.

[5] M. Joham, W. Utschick, and J. A. Nossek, "A symbol rate multi-user downlink beamforming approach for WCDMA," in *Proc. PIMRC*, vol. 2, Sept. 1999, pp. 228–232.

[6] M. Haardt, C. Brunner, and J. A. Nossek, "Joint estimation of 2-D arrival angles, propagation delays, and Doppler frequencies in wireless communications," in *Proc. DSP Workshop*, vol. 1, Aug. 1998, 50, pp. 1–4.

[7] C. Brunner, M. Haardt, and J. A. Nossek, "2-D rake receiver in the space-frequency domain for the uplink of WCDMA," in *Proc. Int. Workshop Intell. Signal Process. Commun. Syst.*, Nov. 1998, pp. 551–555.

[8] C. Farsakh and J. A. Nossek, "Spatial covariance based downlink beamforming in an SDMA mobile radio system," *IEEE Trans. Commun.*, vol. 46, pp. 1497–1506, Nov. 1998.

[9] E. Dahlman, B. Gudmundson, M. Nilsson, and J. Sköld, "UMTS/IMT-2000 based on wideband CDMA," *IEEE Commun. Mag.*, vol. 36, pp. 70–80, Sept. 1998.

[10] E. Nikula, A. Toskala, E. Dahlman, L. Girard, and A. Klein, "FRAMES multiple access for UMTS and IMT-2000," *IEEE Pers. Commun.*, vol. 5, pp. 16–24, Apr. 1998.

[11] F. Adachi, M. Sawahashi, and K. Okawa, "Tree-structured generation of orthogonal spreading codes with different lengths for forward link of DS-CDMA mobile radio," *Electron. Lett.*, vol. 33, no. 1, pp. 27–28, Jan. 1997.

[12] 3rd Generation Partnership Project—3GPP, "Universal Mobile Telecommunications System (UMTS); UTRA (BS) FDD; Radio transmission and reception,", http://www.etsi.org, June 2000.

[13] A. J. Paulraj and C. B. Papadias, "Space-time processing for wireless communications," *IEEE Signal Processing Mag.*, vol. 14, pp. 49–83, Nov. 1997.

[14] L. Bigler, H. P. Lin, S. S. Jeng, and G. Xu, "Experimental direction of arrival and spatial signature measurements at 900 MHz for smart antenna systems," in *Proc. Veh. Technol. Conf.*, vol. 1, July 1995, pp. 55–58.

[15] T. Asté, P. Forster, L. Féty, and S. Mayrargue, "Downlink beamforming avoiding DOA estimation for cellular mobile communications," in *Proc. ICASSP*, May 1998, pp. 3313–3316.

[16] D. Gerlach and A. Paulraj, "Base station transmitting antenna arrays for multipath environments," *Signal Process.*, vol. 54, no. 1, pp. 59–73, Oct. 1996.

[17] 3rd Generation Partnership Project—3GPP, "Universal Mobile Telecommunications System (UMTS); Physical Layer—General Description,", http://www.etsi.org, Mar. 2000.

[18] 3rd Generation Partnership Project—3GPP, "Universal Mobile Telecommunications System (UMTS); Spreading and Modulation (FDD),", http://www.etsi.org, Mar. 2000.

Michael Joham (S'99) received the diploma degree (summa cum laude) in electrical engineering from the Technische Universität (TU) München, Munich, Germany, in 1999. He is currently pursuing the Ph.D. degree at the TU München.

During the summer of 1998 and the summer of 2000, he was a Visiting Research Assistant at Purdue University, West Lafayette, IN. His main research interests are estimation theory and the application of adaptive antennas in mobile communications.

Mr. Joham received the VDE Preis for his diploma thesis.

Wolfgang Utschick (S'93–M'98) completed several industrial education programs before he received his diploma degree (summa cum laude) in electrical engineering in 1993 and the Dr.-Ing. degree (summa cum laude) in 1998, both from the Technische Universität (TU) München, Munich, Germany.

He published a several papers and articles in the field of neural computation, where he studied the design of error-correcting classification systems, and in the field of adaptive array processing, where he focuses on the forward link in wireless communications systems. He is currently a Research Scientist, Industrial Consultant, and Assistant Director of the Signal Processing Research Group at the Institute of Circuit Theory and Signal Processing, TU München. During the summer of 2000, he was a Visiting Research Faculty Member at the Eidgenössische Technische Hochschule, Zürich, Switzerland. His main research interests are signal processing in wireless communications, estimation theory, and nonlinear optimization.